Supplementary Materials

A multiaxial electrical switching of a one-dimensional organic-inorganic (pyrrolidinium)$_2$Cd$_2$I$_6$-ferroelectric photoluminescent

Magdalena Rok[a], Bartosz Zarychta[b], Andrzej Bil[a], Joanna Trojan-Piegza[a], Wojciech Medycki[c], Andrzej Miniewicz[d], Anna Piecha-Bisiorek[a], Agnieszka Ciżman[e], Ryszard Jakubas[a]

[a]Faculty of Chemistry, University of Wroclaw, 14 F. Joliot – Curie, 50-383 Wroclaw, Poland
[b]Faculty of Chemistry, University of Opole, Opole PL-45052, Poland
[c]Institute of Molecular Physics, Polish Academy of Sciences, Smoluchowskiego 17, 60-179 Poznań, Poland
[d] Advanced Materials Engineering and Modelling Group, Faculty of Chemistry, Wroclaw University of Science and Technology, Wybrzeze Wyspianskiego 27, 50-370 Wroclaw, Poland
[e]Department of Experimental Physics, Wrocław University of Science and Technology, Wybrzeże Wyspiańskiego 27, 50–370 Wrocław, Poland

CAPTIONS OF FIGURES

CAPTIONS OF TABLES

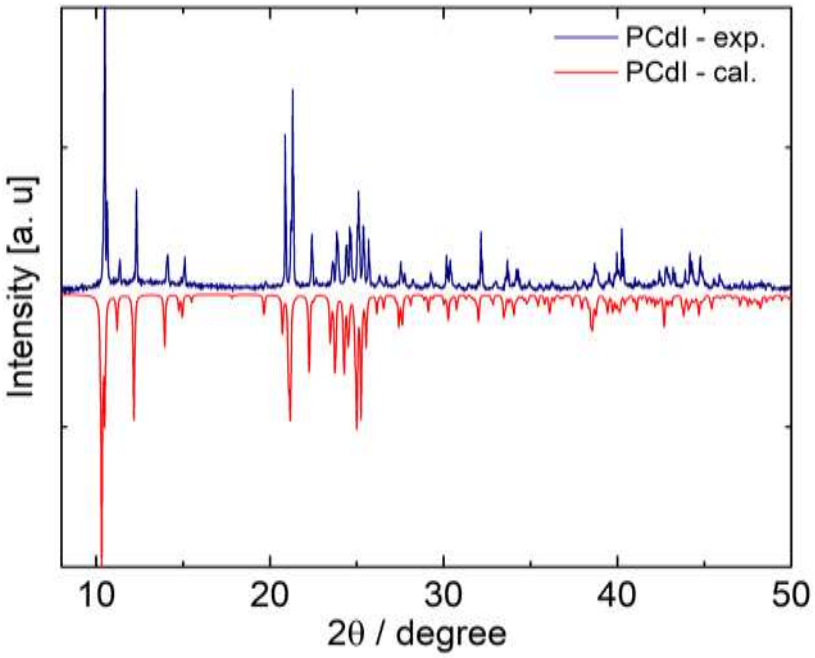

Fig. S1. X-ray diffraction pattern at 298 K of **PCdI** (blue) and calculated from crystal structure (red).

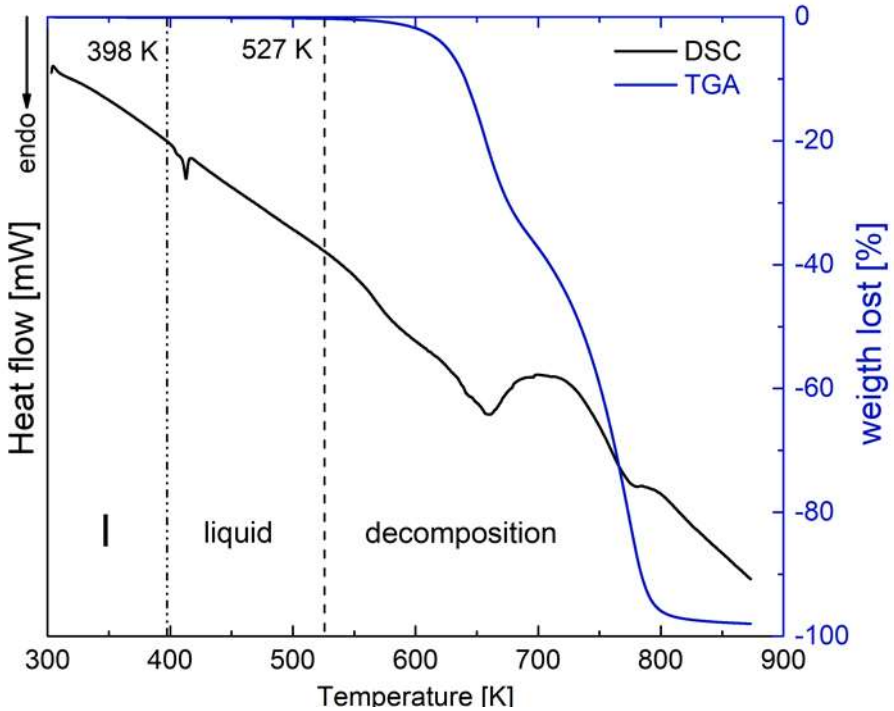

Fig. S2. The results of the simultaneous TGA/DSC analyses for **PCdI** (sample mass m = 13.7640 mg, 5K/min.

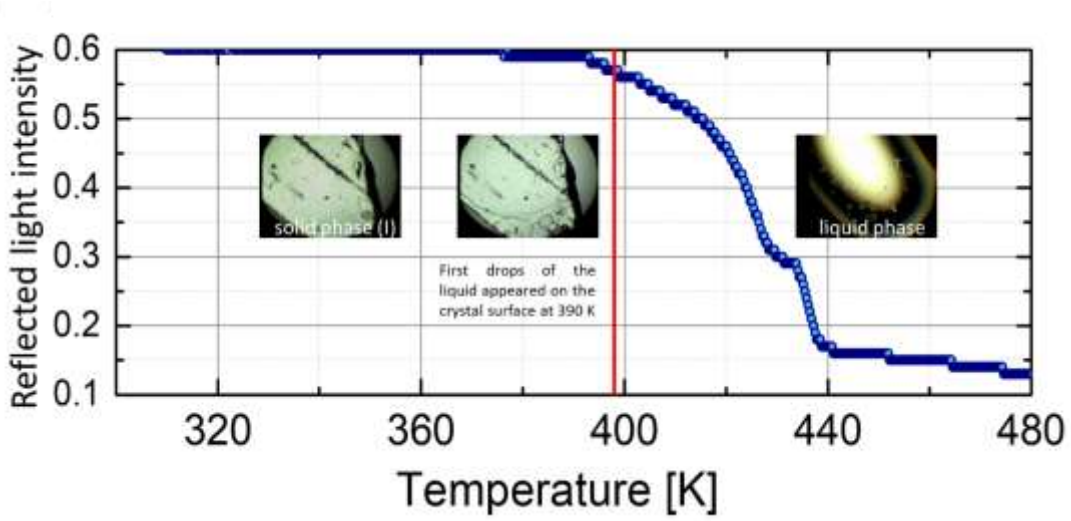

Fig. S3. The melting point measurement of the **PCdI** powder under optical microscope, insert: the photographs of the crystal in two phases, solid I and liquid measured on the heating run.

Table S1. Experimental details. For all structures: $C_8H_{20}Cd_2I_6N_2$ (**PCdI**), M_r = 1130.46, monoclinic, Cc, Z = 4. Experiments were carried out at 100.0 K with Mo Kα radiation. Absorption was corrected for by multi-scan methods, CrysAlis RED, Oxford Diffraction Ltd., Version 1.171.33.57 (release 26-01-2010 CrysAlis171 .NET) (compiled Jan 26 2010,14:36:55) Empirical absorption correction using spherical harmonics, implemented in SCALE3 ABSPACK scaling algorithm.. H-atom parameters were constrained.

	(100K)-II phase	(300K)-I phase
Crystal data		
a, *b*, *c* (Å)	11.6862 (3), 11.7895 (4), 17.2048 (5)	11.9639 (5), 11.9900 (5), 17.3189 (7)
β (°)	93.918 (3)	98.442 (4)
V (Å^3), Z	2364.84 (12)	2457.43 (18)
μ (mm^{-1})	9.62	9.26
Crystal size (mm)	0.56 × 0.40 × 0.27	0.56 × 0.40 × 0.27
Data collection		
Diffractometer	Oxford Diffraction Xcalibur Saphire 2 System	
T_{min}, T_{max}	0.430, 1.000	0.406, 1.000
No. of measured, independent and observed [$I > 2\sigma(I)$] reflections	12855, 5449, 5421	14809, 5786, 4498
R_{int}	0.057	0.060
$(\sin\theta/\lambda)_{max}$ (Å^{-1})	0.660	0.660
Refinement		
$R[F^2 > 2\sigma(F^2)]$, $wR(F^2)$, S	0.036, 0.091, 1.07	0.043, 0.118, 0.99
No. of reflections	5449	5786
No. of parameters	163	236
No. of restraints	2	270
	$w = 1/[\sigma^2(F_o^2) + (0.0603P)^2 + 23.3407P]$ where $P = (F_o^2 + 2F_c^2)/3$	$w = 1/[\sigma^2(F_o^2) + (0.0724P)^2]$ where $P = (F_o^2 + 2F_c^2)/3$
$\Delta\rho_{max}$, $\Delta\rho_{min}$ (e Å^{-3})	1.62, −1.32	1.05, −0.96
Absolute structure	Classical Flack method preferred over Parsons because s.u. lower.	Flack x determined using 1901 quotients [(I+)-(I-)]/[(I+)+(I-)] (Parsons and Flack (2004), Acta Cryst. A60, s61).
Absolute structure parameter	0.15 (6)	0.08 (7)

Computer programs: *CrysAlis CCD* (Oxford Diffraction, 2008), *CrysAlis RED* (Oxford Diffraction, 2008), *SHELXS2013* (Sheldrick, 2015), *SHELXL2013* (Sheldrick, 2015), *SHELXTL* (Sheldrick, 2015). *CrysAlis CCD and CrysAlis RED* 2008, Oxford Diffraction: Oxford Diffraction Ltd, Abingdon, England; Sheldrick GM (2015) Acta Cryst. A71, 3–8.

Table S2. Geometric parameters (Å, º)

100 K		300 K	
Bond lengths			
Cd1—I3	2.7372 (11)	Cd1—I3	2.7168 (18)
Cd1—I2	2.7384 (11)	Cd1—I2	2.7198 (17)
Cd1—I1	2.8391 (11)	Cd1—I1	2.8474 (15)
Cd1—I4	2.8393 (11)	Cd1—I4	2.8504 (14)
Cd2—I5	2.7161 (12)	Cd2—I6	2.7195 (16)
Cd2—I6	2.7373 (11)	Cd2—I5	2.7261 (19)
Cd2—I4	2.8122 (11)	Cd2—I4	2.8337 (15)
Cd2—I1^{i}	2.8747 (11)	Cd2—I1^{i}	2.8502 (15)
I1—Cd2^{ii}	2.8747 (11)	I1—Cd2^{ii}	2.8502 (15)
N1—C5	1.503 (16)	N1—C2A	1.16 (9)
N1—C2	1.504 (18)	N1—C5B	1.48 (10)
C2—C3	1.51 (2)	N1—C5A	1.52 (11)
C3—C4	1.51 (2)	N1—C2B	1.67 (7)
C4—C5	1.49 (2)	C2A—C3A	1.38 (9)
N6—C7	1.526 (16)	C3A—C4A	1.58 (11)
N6—C10	1.527 (15)	C4A—C5A	1.62 (14)
C7—C8	1.525 (19)	C2B—C3B	1.55 (11)
C8—C9	1.52 (2)	C3B—C4B	1.48 (9)
C9—C10	1.495 (18)	C4B—C5B	1.34 (13)
		N6—C7B	1.33 (6)
		N6—C10A	1.34 (6)
		N6—C7A	1.52 (6)
		N6—C10B	1.64 (5)
		C7A—C8A	1.60 (7)
		C8A—C9A	1.49 (7)
		C9A—C10A	1.48 (6)
		C7B—C8B	1.46 (6)
		C8B—C9B	1.51 (7)
		C9B—C10B	1.67 (7)
Valance angles			
I3—Cd1—I2	120.73 (4)	I3—Cd1—I2	121.21 (6)
I3—Cd1—I1	114.76 (4)	I3—Cd1—I1	111.37 (6)
I2—Cd1—I1	106.57 (4)	I2—Cd1—I1	107.68 (6)
I3—Cd1—I4	104.23 (4)	I3—Cd1—I4	107.67 (6)
I2—Cd1—I4	112.29 (4)	I2—Cd1—I4	109.42 (6)
I1—Cd1—I4	95.39 (3)	I1—Cd1—I4	96.72 (4)
I5—Cd2—I6	119.46 (4)	I6—Cd2—I5	118.60 (7)
I5—Cd2—I4	114.49 (4)	I6—Cd2—I4	107.87 (5)
I6—Cd2—I4	108.89 (4)	I5—Cd2—I4	113.89 (6)
I5—Cd2—I1^{i}	105.61 (4)	I6—Cd2—I1^{i}	110.62 (6)
I6—Cd2—I1^{i}	109.97 (4)	I5—Cd2—I1^{i}	107.33 (6)
I4—Cd2—I1^{i}	95.62 (3)	I4—Cd2—I1^{i}	96.24 (5)
Cd1—I1—Cd2^{ii}	96.79 (3)	Cd1—I1—Cd2^{ii}	99.48 (4)
Cd2—I4—Cd1	100.00 (3)	Cd2—I4—Cd1	101.69 (5)
C5—N1—C2	107.3 (10)	C2A—N1—C5A	108 (6)
N1—C2—C3	102.4 (11)	C5B—N1—C2B	92 (5)
C2—C3—C4	103.5 (12)	N1—C2A—C3A	114 (8)
C5—C4—C3	103.2 (12)	C2A—C3A—C4A	102 (6)
C4—C5—N1	106.5 (11)	C3A—C4A—C5A	97 (7)
C7—N6—C10	106.4 (10)	N1—C5A—C4A	102 (7)
C8—C7—N6	103.8 (10)	C3B—C2B—N1	101 (5)
C9—C8—C7	103.5 (10)	C4B—C3B—C2B	100 (7)
C10—C9—C8	101.6 (10)	C5B—C4B—C3B	108 (8)

C9—C10—N6	104.9 (10)	C4B—C5B—N1	118 (7)
		C10A—N6—C7A	115 (3)
		C7B—N6—C10B	121 (3)
		N6—C7A—C8A	102 (4)
		C9A—C8A—C7A	96 (4)
		C10A—C9A—C8A	112 (4)
		N6—C10A—C9A	101 (4)
		N6—C7B—C8B	106 (4)
		C7B—C8B—C9B	111 (4)
		C8B—C9B—C10B	108 (4)
		N6—C10B—C9B	92 (3)
Dihedral angles			
C5—N1—C2—C3	−23.2 (13)	C5A—N1—C2A—C3A	−41 (9)
N1—C2—C3—C4	38.8 (13)	N1—C2A—C3A—C4A	45 (10)
C2—C3—C4—C5	−40.2 (15)	C2A—C3A—C4A—C5A	−25 (9)
C3—C4—C5—N1	25.4 (15)	C2A—N1—C5A—C4A	18 (9)
C2—N1—C5—C4	−1.4 (14)	C3A—C4A—C5A—N1	7 (9)
C10—N6—C7—C8	9.4 (13)	C10A—N6—C7A—C8A	6 (5)
N6—C7—C8—C9	−33.2 (13)	N6—C7A—C8A—C9A	−23 (4)
C7—C8—C9—C10	44.8 (12)	C7A—C8A—C9A—C10A	36 (5)
C8—C9—C10—N6	−38.6 (12)	C7A—N6—C10A—C9A	15 (5)
C7—N6—C10—C9	18.2 (13)	C8A—C9A—C10A—N6	−34 (6)
		C5B—N1—C2B—C3B	−40 (7)
		N1—C2B—C3B—C4B	42 (8)
		C2B—C3B—C4B—C5B	−27 (12)
		C3B—C4B—C5B—N1	−1 (14)
		C2B—N1—C5B—C4B	27 (11)
		C10B—N6—C7B—C8B	7 (6)
		N6—C7B—C8B—C9B	5 (6)
		C7B—C8B—C9B—C10B	−14 (6)
		C7B—N6—C10B—C9B	−14 (5)
		C8B—C9B—C10B—N6	15 (5)

Symmetry code(s): (i) *x*−1/2, *y*−1/2, *z*; (ii) *x*+1/2, *y*+1/2, *z*.

Table S3. Hydrogen-bond parameters.

D—H···*A*	*D*—H (Å)	H···*A* (Å)	*D*···*A* (Å)	*D*—H···*A* (°)
100 K				
N1—H1A···I6	0.97	2.72	3.587 (10)	148.7
N1—H1B···I2^{i}	0.97	3.23	3.724 (11)	113.1
N1—H1B···I3^{ii}	0.97	2.72	3.535 (10)	142.1
C2—H2A···I5	0.97	3.11	4.075 (13)	173.5
C3—H3B···I3^{iii}	0.97	3.23	4.033 (15)	141.7
C5—H5B···I3^{ii}	0.97	3.27	3.840 (13)	119.1
N6—H6A···I3	0.97	2.75	3.575 (11)	143.6
N6—H6A···I5^{iv}	0.97	3.08	3.571 (10)	112.7
N6—H6B···I1^{v}	0.97	3.27	3.802 (10)	116.1
N6—H6B···I2^{v}	0.97	2.72	3.564 (11)	145.1
C8—H8A···I2	0.97	3.18	3.923 (14)	134.3
C8—H8B···I5^{v}	0.97	3.29	3.915 (14)	124.2
C9—H9A···I6	0.97	3.25	3.987 (12)	134.3
C9—H9B···I4^{vi}	0.97	3.31	3.892 (13)	120.4
C9—H9B···I5^{v}	0.97	3.22	3.949 (12)	133.5
C10—H10A···I1^{vi}	0.97	3.22	3.914 (12)	130.1
300 K				
N1—H1A···I3^{ii}	0.97	2.83	3.74 (3)	157.8
N1—H1B···I6	0.97	3.30	4.08 (4)	139.0
C2A—H2AA···I5	0.97	3.07	3.89 (7)	143.3
C2A—H2AB···I6^{iii}	0.97	3.05	3.97 (10)	157.5
C3A—H3AB···I3^{iii}	0.97	3.23	3.94 (8)	131.3
C3A—H3AB···I4^{iii}	0.97	3.28	4.06 (9)	138.3
C2B—H2BB···I5	0.97	2.79	3.71 (7)	159.1
N6—H6A···I2^{v}	0.97	2.77	3.61 (2)	145.7
N6—H6B···I3	0.97	2.82	3.63 (2)	141.9
C8A—H8AA···I2	0.97	3.08	3.95 (5)	149.2
C8A—H8AB···I5^{v}	0.97	3.16	3.95 (5)	139.4
C9A—H9AB···I4^{vi}	0.97	3.33	3.85 (5)	115.8
C10A—H10A···I3	0.97	3.22	3.88 (6)	126.0
C10A—H10B···I1^{vi}	0.97	3.33	3.94 (6)	122.6
C8B—H8BB···I2	0.97	3.16	3.99 (5)	145.1

Symmetry code(s): (i) *x*−1/2, *y*−1/2, *z*; (ii) *x*−1, *y*, *z*; (iii) *x*−1/2, *y*+1/2, *z*; (iv) *x*+1/2, −*y*+1/2, *z*−1/2; (v) *x*, −*y*+1, *z*−1/2; (vi) *x*−1/2, −*y*+1/2, *z*−1/2.

a) b)

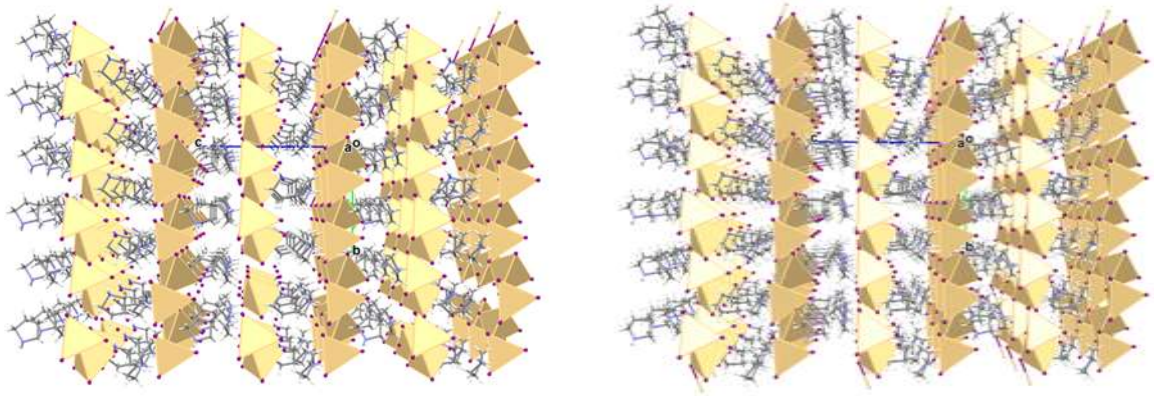

Fig. S4. Packing diagram of (**PCdI**), (a) at 100 K and (b) at 300 K projected at (011) plane

Spontaneous polarization – theoretical calculations.

The Berry phase calculations [1,2] of HT phase were performed using the ordered models of the phase. For this purpose four structures have to be considered, with pyrrolidinium cations set manually to order the phase. Atomic coordinates of the model ordered phases are available in PCdI_300_AA.cif, PCdI_300_AB.cif, PCdI_300_BA.cif and PCdI_300_BB.cif files appended to Supplementary Materials.

Both LDA (Local Density Approximation, Teter Pade parametrization, keyword ixc) [3] and PBE (Perdew, Burke and Ernzerhof) density functionals, [4] as implemented in Abinit, [5,6] were used against plane wave basis sets defined by the energy cut-off of 400 eV.

The pseudopotentials used for these calculations were downloaded from https://www.abinit.org. In case of LDA calculations we used single projector, ordinary norm conserving pseudopotentials based on the Troullier-Martins method [7], generated by D.C. Allan and A. Khein. For PBE calculations the pseudopotentials generated using FHI code were applied.

A dense Monkhorst–Pack k-point grid, ie. 3x3x2 (~ 0.03 $Å^{-1}$) mesh in each direction in the Brillouin zone) was used for electronic structure calculations of both considered phases. [8]

Table S4. Spontaneous polarization [$\mu C \cdot cm^{-2}$] for LT phase and ordered models of HT phase calculated within Berry phase approach using LDA functional. For the polar axes of the LT phase, a polarization indetermination quantum is a multiple of 7.883 $\mu C \cdot cm^{-2}$ along the *a* axis and 11.608 $\mu C \cdot cm^{-2}$ along the *c* axis. The respective values for HT phase are 7.716 $\mu C \cdot cm^{-2}$ and 11.169 $\mu C \cdot cm^{-2}$.

LDA	a	b	c
LT (II)	**-3.184**	**0.000**	**4.582**
HT-AA	-3.691	0.000	5.547
HT-AB	-3.915	0.000	5.776
HT-BA	-3.349	0.001	5.309
HT-BB	-3.578	0.001	5.541
HT (I) – averaged	**-3.633**	**0.000**	**5.543**

Table S5. Spontaneous polarization [$\mu C \cdot cm^{-2}$] for LT phase and ordered models of HT phase calculated within Berry phase approach using PBA functional

PBE	a	b	c
LT	**-3.219**	**0.000**	**4.635**
HT-AA	-3.694	0.000	5.586
HT-AB	-3.917	0.000	5.806
HT-BA	-3.353	0.001	5.375
HT-BB	-3.581	0.001	5.599
HT-averaged	**-3.636**	**0.000**	**5.591**

The numerical data from Tables S4 and S5, representing the components of the spontaneous polarization of phases LT and HT, show little dependence on the density functional selected for the electronic structure calculations.

Due to a polarization indetermination quantum, whose value is determined by crystal cell parameters, accompanying a spontaneous polarization calculated using the Berry phase approach, the obtained results have to be interpreted against the experimental results. In our case it seems plausible to assume that the basic values tabulated in S4 and S5 are of physical significance.

(1) Vanderbilt, D.; King-Smith, R. D. Electric Polarization as a Bulk Quantity and Its Relation to Surface Charge. *Phys. Rev. B* **1993**, *48* (7), 4442–4455.

(2) King-Smith, R. D.; Vanderbilt, D. Theory of Polarization of Crystalline Solids. *Phys. Rev. B* **1993**, *47* (3), 1651–1654.

(3) Ceperley, D. M.; Alder, B. J. Ground State of the Electron Gas by a Stochastic Model. *Phys. Rev. Lett.* **1980**, *45* (7), 566–569.

(4) Perdew, J.; Burke, K.; Ernzerhof, M. Generalized Gradient Approximation Made Simple. *Phys. Rev. Lett.* **1996**, *77* (18), 3865–3868.

(5) Gonze, X.; Beuken, J. M.; Caracas, R.; Detraux, F.; Fuchs, M.; Rignanese, G. M.; Sindic, L.; Verstraete, M.; Zerah, G.; Jollet, F.; et al. First-Principles Computation of Material Properties: The ABINIT Software Project. *Comput. Mater. Sci.* **2002**, *25* (3), 478–492.

(6) Gonze, X.; Jollet, F.; Abreu Araujo, F.; Adams, D.; Amadon, B.; Applencourt, T.; Audouze, C.; Beuken, J. M.; Bieder, J.; Bokhanchuk, A.; et al. Recent Developments in the ABINIT Software Package. *Comput. Phys. Commun.* **2016**, *205*, 106–131.

(7) Troullier, N.; Martins, J. L. Efficient Pseudopotentials for Plane-Wave Calculations. II. Operators for Fast Iterative Diagonalization. *Phys. Rev. B* **1991**, *43* (11), 8861–8869.

(8) Monkhorst, H. J.; Pack, J. D. Special Points for Brillouin-Zone Integrations. *Phys. Rev. B* **1976**, *13* (12), 5188–5192.

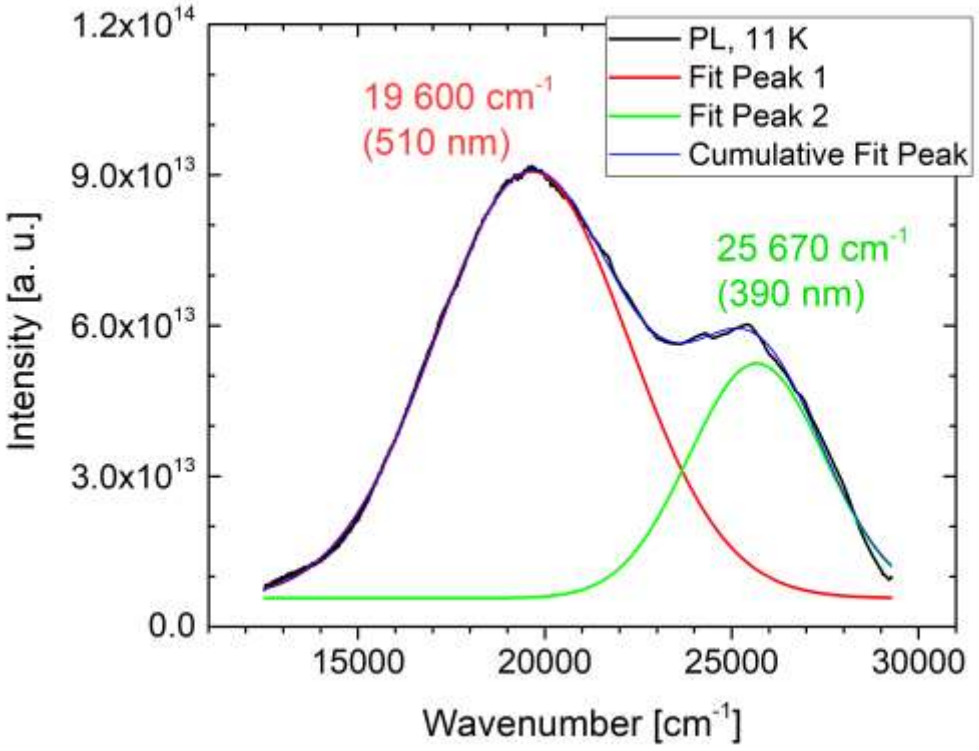

Fig. S5. Gaussian deconvolution of photoluminescence spectrum of **PCdI** measured at 11 K.

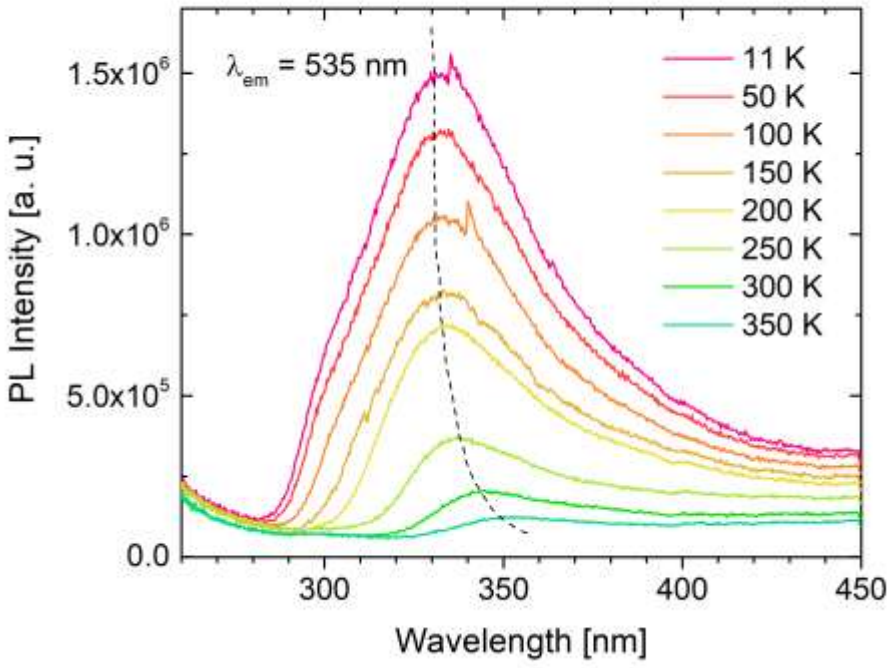

Fig. S6. Temperature dependence of excitation spectra monitored at 535 nm.

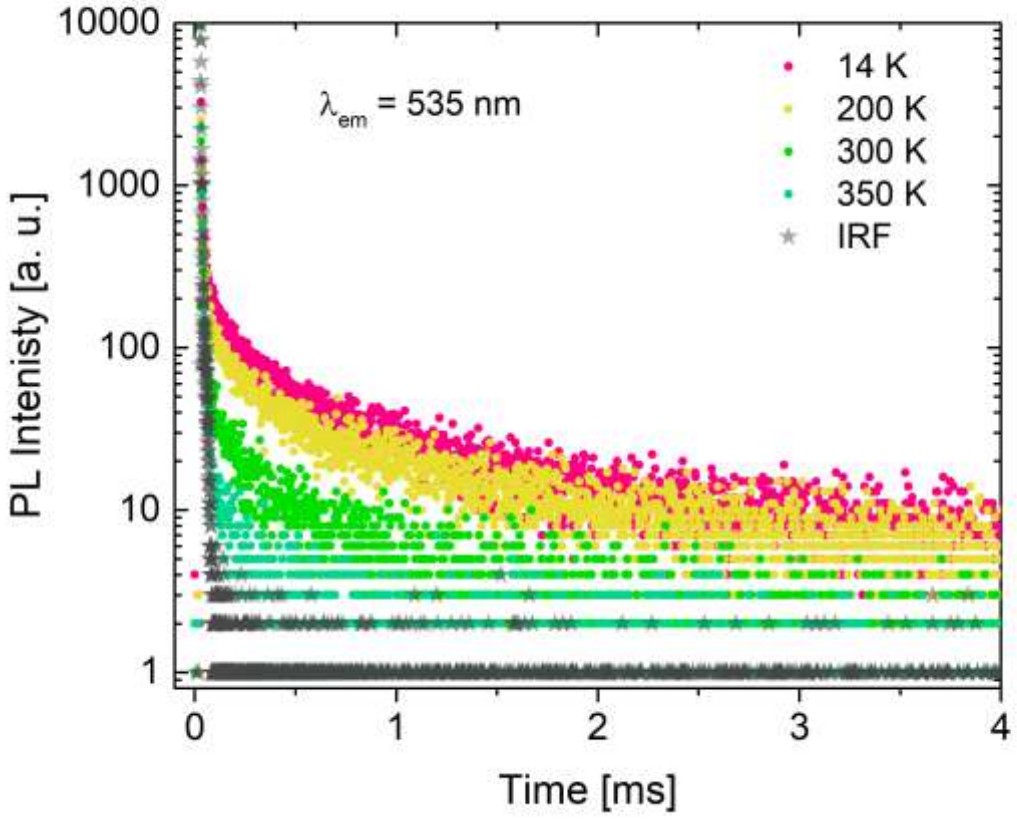

Fig. S7. Temperature dependence of 535 nm emission decay.

Table S6. Temperature dependence of average lifetime of 535 nm emission. The decay curves recorded during 335 nm excitation.

Temperature [K]	τ_{av} [µs]
11	490
50	512
100	555
150	522
200	521
250	276
300	132
350	12

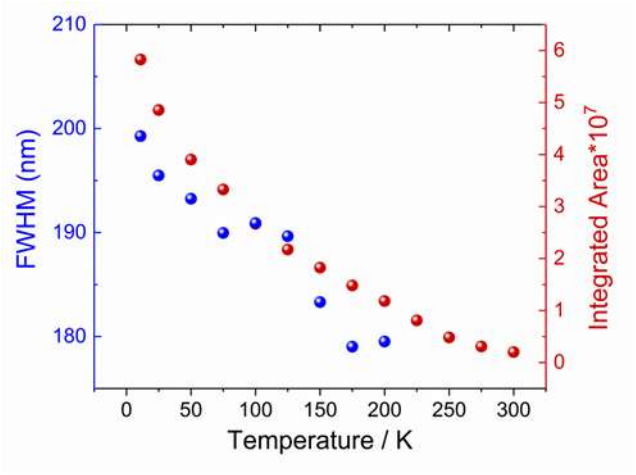

Fig. S8. Temperature dependence of the integrated emission intensity (brown spheres) and FWHM (blue spheres) of **PCdI**.

Table S7. Comparison of the CIE chromaticity coordinates (x, y) and CCT (K) for **PCdI**.

ID	1931 Measurements	X Coord	Y Coord	I (lum)	CCT [K]
1	Em 25.0K (TempMap)	0.30117	0.37488	3.340E+004	6733
2	Em 50.0K (TempMap)	0.29657	0.37205	2.653E+004	6955
3	Em 75.0K (TempMap)	0.29513	0.37200	2.262E+004	7020
4	Em 100.0K (TempMap)	0.29517	0.37217	1.854E+004	7017
5	Em 125.0K (TempMap)	0.29742	0.37518	1.568E+004	6893
6	Em 150.0K (TempMap)	0.29910	0.38024	1.354E+004	6783
7	Em 175.0K (TempMap)	0.30207	0.38574	1.128E+004	6626
8	Em 200.0K (TempMap)	0.30163	0.38472	8.945E+003	6650
9	Em 225.0K (TempMap)	0.30183	0.38049	5.986E+003	6668
10	Em 250.0K (TempMap)	0.30507	0.37685	3.511E+003	6557
11	Em 275.0K (TempMap)	0.30790	0.38042	2.294E+003	6423
12	Em 300.0K (TempMap)	0.30577	0.37397	1.474E+003	6545

^{1}H-NMR.

Temperature dependence of the second moment (M_2) of the ^{1}H NMR line for **PCdI** is shown in Figure S9. It should be noticed that even at the lowest temperatures (113 K) any plateau of M_2 has been not reached. Two reductions of the M_2 value are visible. First reduction of $\Delta M_2(1)$, is only partially visible above 113 K and the next one , $\Delta M_2(2)$, occurs around 230 K. Between 230 and 290 K M_2 value stabilizes at about 8.4 G^2. It means that the full isotropic motion of the pyrrolidinium cation is not expected even at RT. A similar behaviour of the M_2 and comparable values (M_2) were found in another pyrrolidinium analogues [1, 2].

The basic equation for the dipolar second moment, M_2, of a NMR line was derived by van Vleck [3]:

$$M_2 = \frac{3}{5} I(I+1)\gamma^2\hbar^2 \frac{1}{N} \sum_{i=1}^{N} \sum_{j=1}^{N} R_{ij}^6 \qquad (1)$$

where N is the number of protons in the unit cell. The rigid value of M_2 calculated from the crystal structure of **PCdI** appeared to be about 19,9 G^2 with assumed lengths of bonds: C-H 1.09 Å and N-H 1.03 Å. The obtained from the theoretical calculation M_2 value is much smaller than the measured one. Such a discrepancy is probably the result of uncertainty in adopting the correct N-H bond lengths. Analysis of the temperature dependence of M_2 can be performed on the basis of the BPP formula:

$$\mathrm{M_2} = \Delta\mathrm{M_2}(1)\tfrac{2}{\pi}\tan^{-1}(\gamma_H\tau_c\sqrt{\mathrm{M}_2}) + \Delta\mathrm{M_2}(2)\tfrac{2}{\pi}\tan^{-1}(\gamma_H\tau_c\sqrt{\mathrm{M}_2}) + \mathrm{M_2^{Motion}} \qquad (2)$$

where $\tau_c = \tau_0\, exp(E_a/RT)$, M_2^{Rigid} (where $M_2^{Rigid}=\Delta M_2(1)+\Delta M_2(2)+M_2^{\mathrm{Motion}}$) and M_2^{Motion} are the second-moment values before and after of both second moment reduction, respectively

Based on the equation (1) and (2) the following results we obtained : for the first reduction of M_2 the activation energy (E_{a1}) = 12.1 kJ/mol and the correlation time (τ_1) = 5.88 10^{-11} s, whereas for the second reduction of M_2 the E_{a2}= 14.9 kJ/mol and τ_2 = 2.09 10^{-9} s.

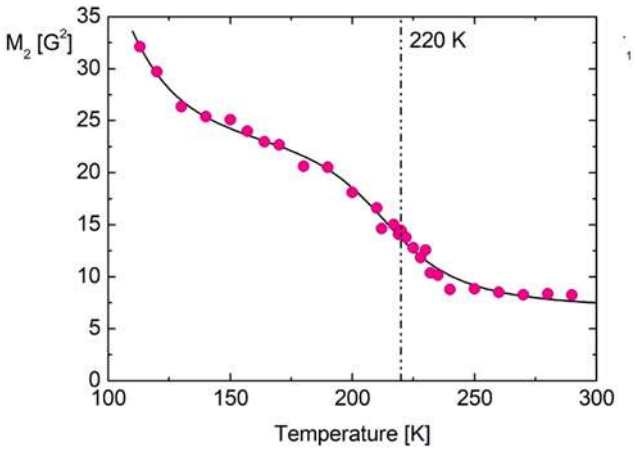

Fig. S9. Temperature dependence of the second moment, M_2, of the proton NMR lines for **PCdI**.

Table S8. Activation energies, correlation times and motional constants evaluated for **PCdI.**

Temperature Range [K]	Component	E_a [kJ/mol]	τ_0 [s]	C [s^{-2}]
90 - 170	1	6.1	$2.5\ 10^{-11}$	$2.6\ 10^{7}$
170 - 226	2	32.2	-	-
226 - 230	3	34.3	-	-
230 - 239	4	16	-	-
259 - 296	5	17.5	-	-

[1] M. Wojciechowska, A. Gagor, A. Piecha-Bisiorek, R. Jakubas, A. Cizman, J. K. Zaręba, M. Nyk, P. Zieliński, W. Medycki and A. Bil, *Chem. Mater.*, 2018, **30**, 4597–4608.

[2] M. Ksiadzyna, A. Gagor, A. Piecha-Bisiorek, A. Cizman, W. Medycki and R. Jakubas, *J. Mater. Chem. C*, 2019, **7**, 10360–10370.

[3] Van Vleck, J. H. Dipolar Broadening. *Phys. Rev.* **1948**, *74*, 1168–1183.